Powder Technology 413 (2023) 118016

Contents lists available at ScienceDirect

Powder Technology

journal homepage: www.journals.elsevier.com/powder-technology

Disk-shaped compact tension test for fracture analysis on pharmaceutical tablets

J. Girardot [a], J.B. Kopp [a], B. Croquelois [b], P. Tchoreloff [b], S. Morel [b], V. Mazel [b,*]

[a] Arts et Metiers Institute of Technology, CNRS, I2M Bordeaux, France
[b] University of Bordeaux, CNRS, I2M Bordeaux, France

GRAPHICAL ABSTRACT

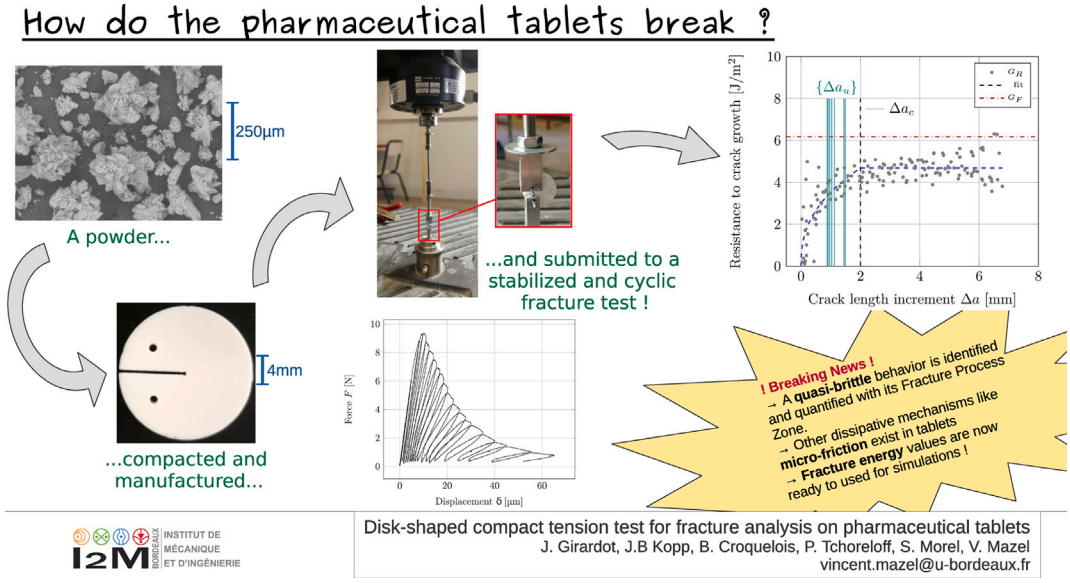

HIGHLIGHTS

- Fracture behavior of pharmaceutical tablets is a key issue for their manufacturing.
- An alternative to the diametral compression test is proposed here.
- No instability issues using the notch opening displacement controller.
- A quasi-brittle behavior identified through equivalent LEFM theory.
- Presence of dissipative mechanisms like micro-friction inside the process zone.

ARTICLE INFO

Keywords:
DCT
Pharmaceutical tablet

ABSTRACT

Pharmaceutical tablets must meet a number of requirements and among them, the mechanical strength plays an important role. The diametral compression test is generally used to evaluate it but can generate unstable failures. Thanks to load–unload cycles applied to the tablets subjected to a DCT test, it was shown that the

* Corresponding author.
E-mail address: vincent.mazel@u-bordeaux.fr (V. Mazel).

https://doi.org/10.1016/j.powtec.2022.118016
Received 12 July 2022; Received in revised form 28 August 2022; Accepted 8 October 2022
Available online 18 October 2022

Quasi-brittle fracture
Energy release rate
Fracture process zone
L.E.F.M. equivalent
R-curve

concept of equivalent linear elastic fracture mechanics usually, can be successfully applied to the Mode I fracture behavior. Within this framework, the equivalent elastic crack growth resistance, commonly called resistance curve (R-curve), of the studied material was obtained and revealed the development of a Fracture Process Zone (FPZ) which is symptomatic of a quasi-brittle behavior. Moreover, the cyclic loading applied during the fracture test revealed the existence of a second dissipative mechanism leading to residual crack opening which seems to be mainly caused by friction phenomenon in the FPZ.

1. Introduction

Pharmaceutical tablets are common forms of drug delivery systems. They are produced using a process of die compaction. Compared to the die compaction used in other fields (e.g. ceramics or metallic powders), the specificity of pharmaceutical die compaction, also called tableting, is the use of relatively high strain rates. The time of compression of the powder in the rotary presses used in the industry is around a few 10 ms. This makes it possible to produce several hundred thousand tablets per hour and this explains the wide use of this process in the pharmaceutical industry [1].

Despite these advantages, tableting can also be a challenging process and several kinds of defects can appear during the manufacturing of tablets. Among these defects, problems of tablet fracture are commonly reported. In some conditions, the tablet breaks when ejected from the die. Depending the kind of failure, these phenomena are called capping or lamination [1]. There is a large literature on this subject, and the mechanisms that promote the failure have been proposed [2–8]. Nevertheless, these phenomena are still complicated to predict. One of the reason is that the fracture behavior of tablets is still not fully understood.

Depending on the chemical nature of the powder used to make the tablets, the fracture behavior obtained can differ. Some products, like microcrystalline cellulose, are said to present a ductile failure whereas other products, like lactose, mannitol or calcium phosphate seems to present brittle fracture [3,9,10]. Hiestand et al. proposed a classification based on the Brittle Fracture Index (BFI) coefficient [3]. It consists on using the maximum force evaluated on a brazillian test for a drilled and non drilled specimen, respectively F_{t0} and F_t in the following equation:

$$\mathrm{BFI} = \frac{1}{2}\left(\frac{F_t}{F_{t0}} - 1\right). \tag{1}$$

The brittle fracture index was developed in order to classify the materials related to their ability to relax local stresses and then predict defects like capping and lamination. Results presented in the literature indicate that products with a high BFI, i.e. that present a brittle fracture, are more prone to present capping and lamination during compaction. The BFI is obtained by calculating the apparent tensile strength of tablets with and without a hole at the center, from the peak force obtained in the diametral compression test, also known as the brazilian test.

The brazillian test is a common way (Fig. 1-a), for many decades, to evaluate the tensile strength of heterogeneous and brittle materials like rock [11–14], concrete [15], ceramics [16–19] and pharmaceutical tablets [20–22]. This mechanical test presents great advantages compared to the bending test regarding the experimental set up, especially for pharmaceutical tablets which are mainly cylindrical and cannot be easily manufactured in the shape adapted to other tests. Nevertheless, strong recommendations need to be followed in the setting up of this test to avoid contact boundary effects [23–25].

These limitations do not make it possible to obtain a quantitative characterization of the fracture behavior using this test. For example, it is well-known that different tensile strengths are obtained in the Brazilian test and in the three-point bending test [26–29]. Nevertheless, no convincing explanation of this phenomenon is so far proposed in the literature.

A pharmaceutical tablet is a porous and heterogeneous solid. Recent works proposed to link these inherent defects of the material and the strength evaluation through standard brazillian tests [30]. An extended Hiestand criteria was also proposed [31] and seemed to indicate that the behavior of pharmaceutical materials may be better described as a quasi-brittle material than as a brittle one.

The quasi-brittle theory was mainly used for concrete-like materials [32–35]. In a quasi-brittle material, the tip of the main crack originates from a finite Fracture Process Zone (FPZ) in which toughening mechanisms take place as microcracking and crack bridging. When a fracture test is performed on a notched specimen, the FPZ develops from the notch up to a critical size, then the main crack propagates preceded by its critical FPZ, leading the so-called self-similar propagation regime. Nevertheless, for most specimen geometries, the self-similar propagation of the main crack takes place in the postpeak regime emphasizing that, at peak load, the FPZ is still under development. Thus, studying the fracture behavior from the peak load leads to a very partial characterization of the fracture phenomena. It is thus necessary to use a fracture test that makes it possible to study the whole fracture process, *i.e.* the pre- and post-peak phenomena. Moreover, in such materials, the Linear Elastic Fracture Mechanics (LEFM) cannot be used directly due to the existence of the FPZ ahead of the main crack tip and the associated non linear phenomena.

The concept of equivalent linear elastic fracture mechanics was developed in the literature in order to apply the tools of LEFM to quasi-brittle materials [36–39]. It is also known that energy dissipative mechanisms due to internal contacts and friction phenomena which take place within the FPZ need to be taken into account through cyclic loading [33], in order to avoid overestimation of the energy release rate.

In the pharmaceutical field, some studies used the Single Edged Notched Beam (SNEB) test (Fig. 1-b) [40,41]. Nevertheless, this test limits the free development of the FPZ or the self-similar propagation of the main crack due to the compression zone which is present along the specimen ligament. Thus, if this test is suited to study a brittle material, it does not allow for a correct study of quasi-brittle materials unless using large dimensions (which is difficult for pharmaceutical powder-based materials).

To overcome these problems, it is proposed in this article to use the Disk-shaped Compact Tension (DCT) test which proposes, like all the previous works, an opening fracture mode, so called `mode I`, opposed to the two other opening modes `II` and `III`, the transverse and longitudinal shear opening modes. This test is well known as a natural self-stabilized fracture test [42] and was used successfully for a quasi-brittle material such as concrete [43]. This test presents many advantages. First, thanks to a retroaction loop on the displacement measurement, it is possible to control the propagation of the crack and thus to avoid any dynamic uncontrolled propagation that would require a dynamic fracture approach [44]. Second, this test allows for a good control of the boundary conditions. Finally, it can be applied to the geometry of a tablet (round) which is close to the geometry used industrially and that can be manufactured using relevant compaction conditions. The objective of this work was to show, on one model material, that the DCT test can be applied to pharmaceutical tablets and that it makes it possible to study their quasi-brittle behavior.

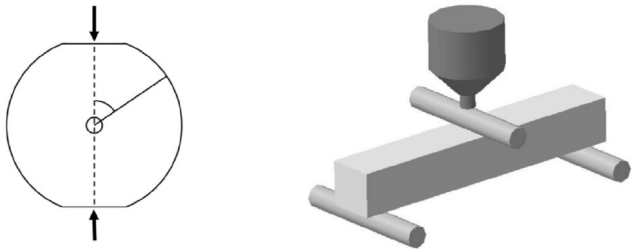

(a) (b)

Fig. 1. The two main test used in the pharmaceutical field: the brazilian test [30] (a) and the SENB test [40] (b).

2. Material and tools

2.1. Tablets manufacturing

2.1.1. Powders

The powder used to produce compacts in this study was an anhydrous calcium phosphate (ACP) (Anhydrous Emcompress®, JRS Pharma, Rosenberg, Germany). Fig. 2 presents, for this product, the particle size distribution data (analysis performed in dry mode at 0.5 bars by laser diffraction using a Mastersizer 2000 Malvern, Malvern, UK) and a micrography obtained using a scanning electron microscope (TM3000, Hitachi, Tokyo, Japan). The mean grain size of the ACP powder was found close to 173 µm. To perform the compaction experiments, the product was mixed with 1.5% (w/w) of magnesium stearate (Cooper, Melun, France) to minimize the frictions in the die. The blending was performed at 49 rpm for 5 min using a turbula mixer (Type T2C, Willy A Bachofen, Muttenz, Switzerland).

2.1.2. Tablet compaction

All the compacts were produced using a compaction simulator *Stylcam*® (Medelpharm, Beynost, France). This tableting press is a single station press. It is equipped with force sensors (accuracy of 10 N) and the displacements of the punches are monitored with an accuracy of 0.01 mm.

One set of round flat-faced euro B punches with a diameter of 16 mm was used (ACM, Avilly-Saint-Leonard, France). All the compacts were obtained using the same compaction kinematic (total compression time of about 100 ms). The compression profile used on the stylcam was a direct cam profile running at 15cpm. An example of the obtained kinematic can be found on Fig. 3.

One compression pressure of 200 MPa was chosen for the selected product in order to obtain sufficiently strong tablets to perform the tests. The filling height was set in order to obtain tablets with a thickness around 4.6 mm.

2.1.3. Tablet machining

The cylindrical tablets were then modified in order to obtain the DCT geometry presented in Fig. 4. Two holes for tensile loading of the specimen and an initial notch were machined. In the pharmaceutical field, two techniques are used to insert holes in the compacts: using specially designed punches [3,45–47] or machining holes using a drill [30,48]. In the present study, the last method which was already successfully applied in the case of pharmaceutical tablets was used. It is already known that this process does not damage the sample near the hole [30]. A micro-chainsaw with a $e = 0.5$ mm width disk was used to machine the initial notch and its length was the half of the diameter as $D = 8$ mm. The two holes, with a diameter D_p of 1 mm, were machined for the pins using a specific drill bit. The position of the pins and of the tip of the initial notch were set such that the ratio a_0/W was equal to 0.35. The final geometry of the sample does not follow the standard ASTM (E 399 – 90), but remains closed to it.

2.2. Experimental setup

The implementation of this test required the development of an experimental device illustrated in Fig. 5. As can be seen, the upper part of the sample is connected to a conventional tension-compression machine MTS of 50 kN capacity thanks to a pin and an "extra-flexible" steel wire of 3 mm diameter, allowing the rotation of the sample to its optimal position during the loading. A system of nut/counter-nut ensured an optimal positioning of the device. The lower part of the device was fixed to the machine frame to avoid any unwanted rotation during the unloading phases. To measure the force, a 100 N load cell was used. For the displacement measurement, a digital extensometry system was used with two cameras (one for each side of the sample). Based on the movement of a fresh speckle applied on both sides of the sample, the value of the displacement measured by each extensometer (using the Vic2D software) corresponded to the relative displacement between two small area of interests (the pink squares in Fig. 5-(b)) located in the alignment of the pins, on both sides of the initial notch and in the immediate vicinity of the pins. Note that the average of these displacements led to an estimation of the displacement corresponding to the load applied to the specimen and also to the external work. Indeed, this displacement avoids the consideration of indentation displacements due to the pin contacts with the specimen and hence provides a reliable estimation of the actual load displacement implied in the external work done on the specimen. The spatial resolution of the two cameras is 1 pixel for 15 µm, the precision of the two extensometers being around one twentieth of a pixel, this is equivalent in our case to an accuracy of about 0.7 µm.

During the loading and the unloading, the specimen was stressed in tension (Mode I) by imposing a crack opening speed controlled by the digital extensometry. A proportional–integral–derivative (PID) controller was adjusted between the displacement of the machine (*i.e* the displacement of the upper pin) and the optically measured displacement. It ensured a real time control of the crack opening and stabilized the crack propagation. The loading rate, *i.e.* the notch opening velocity, was set equal to $0.5\,\mu m\,s^{-1}$ for all tests in this work. The next section illustrates this stability control.

3. Preliminaries

3.1. Stability during monotonic loadings

A monotonic DCT test was first performed using a constant cross head displacement velocity (*i.e.* without notch opening control). The force–displacement curve is shown in Fig. 6. A sudden break of the specimen occurs just after reaching the maximum force at around 9 N.

Fig. 7 exhibits the load–displacement response obtained from the same experimental set up but by controlling the test in displacement from the notch opening measured using the average of the two digital extensometers. The curve exhibits first a linear portion corresponding to the elastic regime of the specimen until reaching also a maximum value around 9 N. Then a non linear behavior takes place up to the peak load followed by a post peak regime in which the load decreases progressively with respect to the notch opening displacement. The non linear regime occurring in the pre-peak regime and continuing in the post-peak, as shown in Fig. 7, is symptomatic of a softening behavior as expected in the case of a quasi-brittle behavior and is not observable without the notch opening controller. This softening behavior is associated with the development of the FPZ from the initial notch in which microcracking and crack bridging phenomena take place.

Thus, the behavior exhibited by the tablet was typical from a quasi-brittle material and it proved that the material used must be treated as such. It confirms that, if the maximum force obtained from a brazilian test is sufficient to characterize a brittle behavior, this one appears very insufficient to characterize the complexity of a quasi-brittle fracture

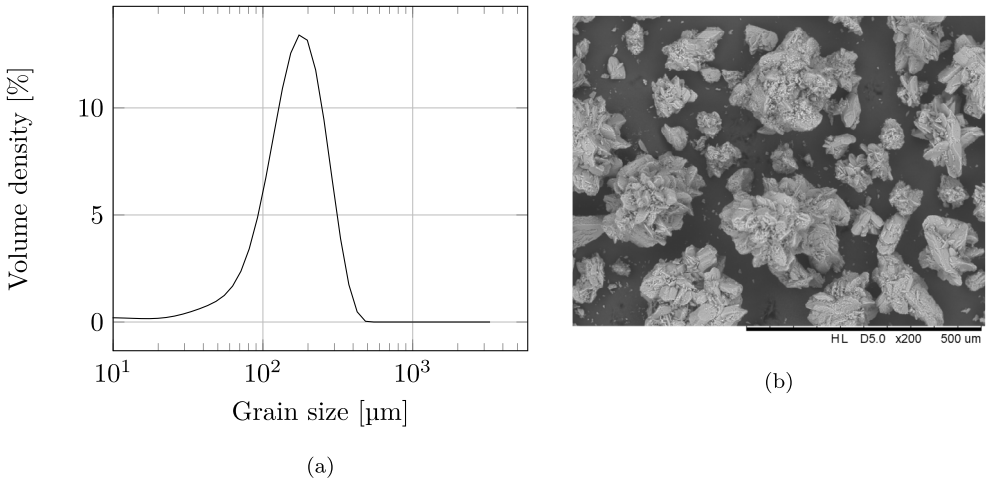

Fig. 2. Granulometry (a) and microscopy of the powder (b).

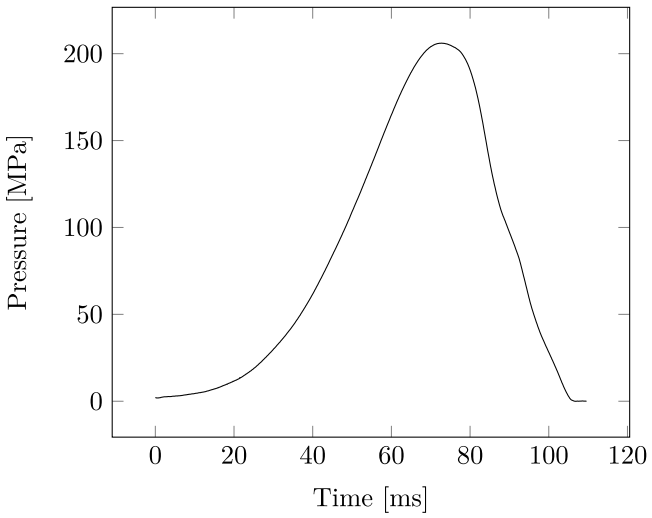

Fig. 3. Compaction kinematic used to obtain the compress..

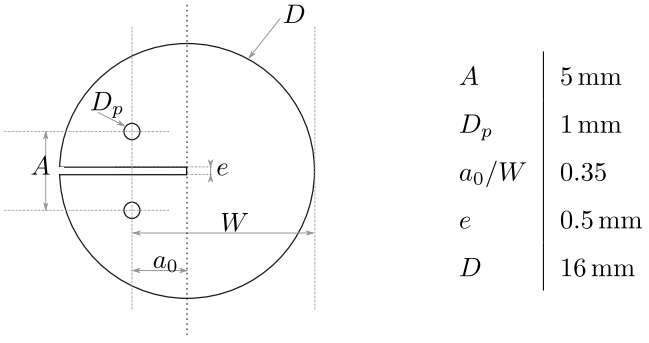

A	5 mm
D_p	1 mm
a_0/W	0.35
e	0.5 mm
D	16 mm

Fig. 4. Sample geometry schemes for the DCT test (the width w is 4.6 mm).

process induced by the development of a fracture process zone. Indeed, if the characterization of a brittle material requires the estimate of a single fracture energy value which can be obtained from the peak load, the characterization of a quasi-brittle fracture process requires the estimate of the resistance to crack growth with respect to the crack advance.

If the monotonic loading test allows the observation of the quasi-brittle behavior of the material, it appeared insufficient to ensure that the crack propagation only involves dissipation of elastic energy which would then be characterized by a simple decrease of the elastic stiffness of the specimen and that no energy was dissipated through other dissipative phenomena. In order to analyze this last point, cyclic loading tests are necessary and are presented in the next section.

3.2. Cyclic loadings

A progressive cyclic displacement was then applied on eight samples. The boundary conditions remained the same as for the monotonic test with a notch opening control and a progressive displacement was imposed on the specimen. The loading was divided into 20 cycles. The load–displacement response is plotted in Fig. 8 and is compared to the result shown in Fig. 7. The envelope curve of the cyclic loading is comparable to the response obtained from the monotonic curve which was expected and makes it possible to show that the test was properly controlled and repeatable.

Moreover, cyclic tests can be used to check if residual displacements are cumulated during the cycles. This can be done by measuring, for each cycle noted i, the residual displacement using the reloading curve of the following cycle $i + 1$. When the sample is reloaded for the cycle $i + 1$, the initial linear slope corresponds to the current stiffness of the sample. When a straight line is fitted into this linear part, if the process is completely elastic, it should intercept the origin. Indeed, if the FPZ development only involved toughening mechanisms such as microcracking and crack bridging associated or not with the propagation of the main crack, the elastic released energy should only lead to a decrease of the elastic stiffness of the specimen without any residual displacements. Thus, if the line intercepts the x-axis at a positive value, this value would be symptomatic of a residual displacement and reveal that some energy was dissipated by other mechanisms like microfriction (or micro-plasticity). The results of this evaluation are presented in the following Fig. 9.

The cumulated residual displacement was increasing for all the tested samples, starting at 0 and reaching values between 10 and 40 µm. The high difference on the values at the end of the cycles can be explained by the natural variability of the microstructure of the material and also with the graphical building of the elastic stiffness which can induce also a variability regarding the intersection with the x-axis. Nevertheless, among all the eight tests, the tendency was clear and the residual displacement was increasing during the crack propagation and thus ACP cannot be considered as a purely damageable elastic material. This means that the secant stiffness cannot be used to estimate the elastic stiffness of the specimen and hence to estimate the equivalent linear elastic crack length used as the x-axis of the R-curve.

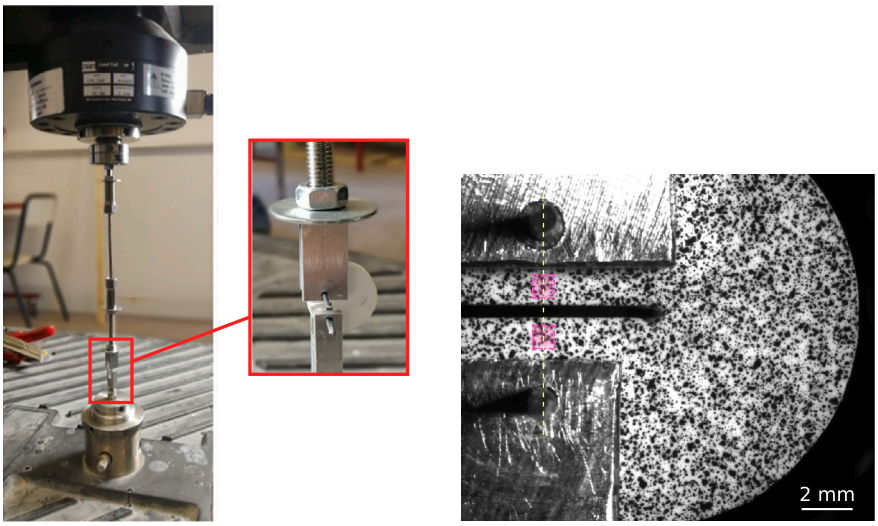

Fig. 5. Pictures of the experimental set up with a sample without the speckle (a) and details of one side of the speckle used for the digital extensometers where pink squares are the area of interest (b). These areas are aligned with the pin axis, on both sides of the initial notch and in immediate vicinity of the pin axis. The relative displacement between the areas of interest was used for the displacement control of the test.

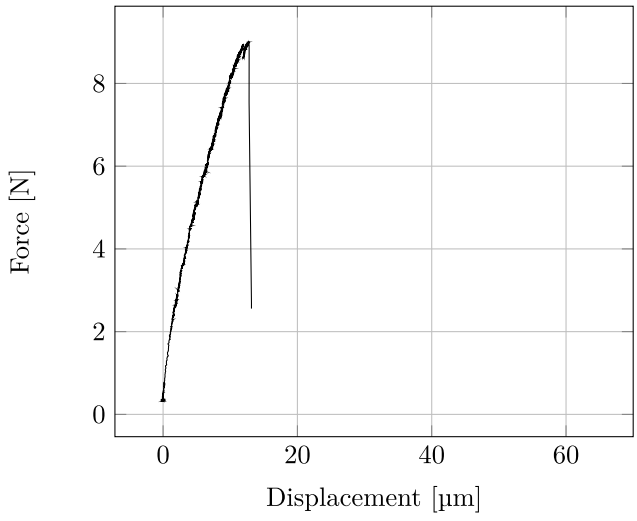

Fig. 6. Typical load–displacement curve obtained from a non-stabilized monotonic loading (sample #A).

In this sense, the fracture energy $G_F \approx 6.17\ \mathrm{J\,m^{-2}}$ estimated from the area under the red envelope curve plotted in Fig. 8 integrates both the actual fracture energy of the tablet and the energy related to the microfriction mechanism accompanying the fracture phenomena. As a consequence, in the rest of this work, only cyclic tests were considered.

A specific analysis was required to dissociate the actual fracture energy and the energy related to other dissipative mechanisms. One could speak of *plasticity* because of the residual displacement. This term might seem abusive from the point of view of the local mechanisms which are not *a priori* associated with plasticity, but rather than with microfriction phenomenon as previously mentioned. Nevertheless, the term *plasticity* was used in the rest of this article.

3.3. Analysis procedure

3.3.1. Elastic stiffness

The graphical procedure applied from the load–displacement curve to get the elastic stiffness of each cycle is illustrated in Fig. 10. For each cycle, a red line is built thanks to a linear regression and corresponds to the tangent of the curve. The minimal mean square error is used to quantify the proper range of the load–displacement curve that is set to evaluate the tangent. Non linear behaviors appear at the beginning of the reloading part of the cycle, mainly due to contact effects and/or microfriction mechanisms. On Fig. 10, the slope of the red line corresponds to the elastic stiffness of the sample at the onset each cycles.

3.3.2. Energetic evaluation

In order to dissociate the energies related to fracture from other dissipative mechanisms at each cycle, the following method was proposed for two consecutive cycles i and $i+1$ and is also illustrated in Fig. 10 (cycles number 6–7 and number 15–16 on the cyclic DCT test of the sample referred to #3):

- the *orange* area was used as the elastic energy loss by quasi-brittle damage. To evaluate graphically this area, two lines L1 and L2 (in red in Fig. 10-a) was defined that are respectively the slope of the elastic stiffness of cycles i and $i+1$. Then, the point P1 was defined as the peak force during the cycle i. And finally, the point P2 was defined as the intersection between : (1) L2′ which is parallel to L2 and have the same origin than L1, and (2) the force ordinate when the unloading of the cycle i is beginning. Finally, the orange area was evaluated with the following contour {L1;P1;P2;L2′};
- the *blue* area was used as the plastic energy. To evaluate graphically this area, the orange area was subtracted from the total area composed of the contour {L1;`part of the curve between` L1 `and` L2;L2}.

The so-called ‘elastic’ and ‘plastic’ energies were estimated from the orange and blue surfaces. These energies was used to estimate the resistance to crack growth of the tablets also called as resistance curve or R-curve.

3.3.3. Equivalent LEFM crack length

In order to estimate the resistance curve of the material, the equivalent LEFM formalism was used. In our case, as seen in the previous section, an energetic approach was considered. In quasi-brittle fracture, the development of FPZ ahead of the crack tip prohibits the direct use of LEFM because of:

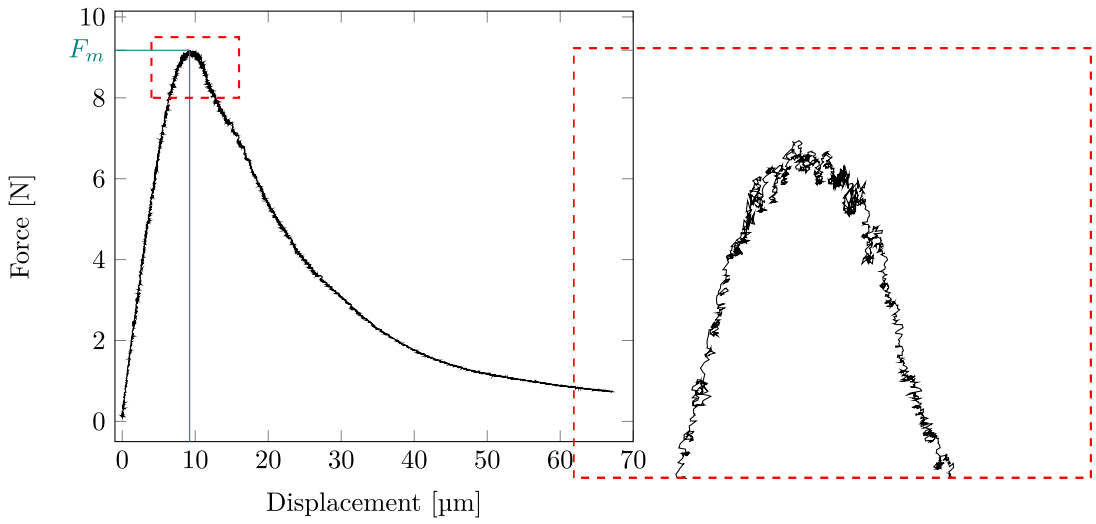

Fig. 7. Typical load–displacement curve obtained from a monotonic loading preformed under notch opening control (sample #B). The term F_m corresponds to the maximum force during the test.

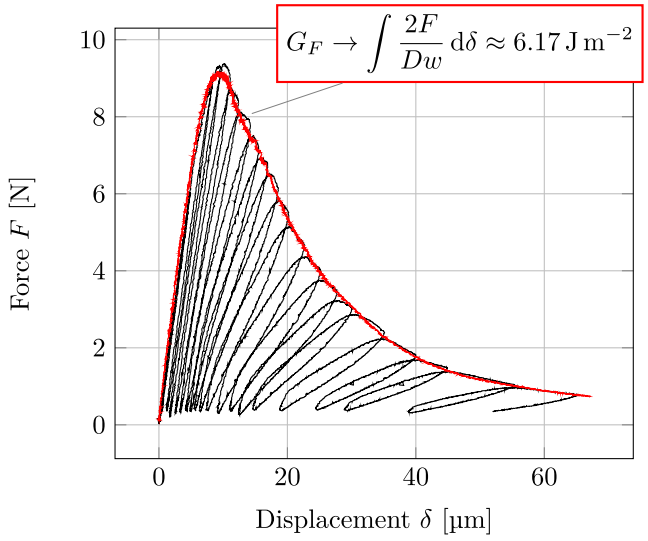

Fig. 8. Typical force–displacement curve for a cyclic loading (sample #8). The superposed red curve is the previous monotonic test (sample #B) for comparison.

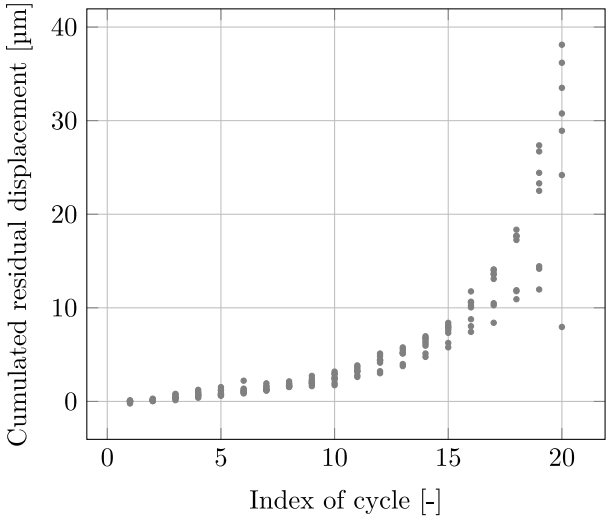

Fig. 9. Experimental results for the cumulated residual displacement for all the 8 sample tested in this work.

- non linear toughening mechanisms taking place in the FPZ;
- the difficulty to estimate the location of the crack tip in the FPZ.

Nevertheless, an adaptation of LEFM so called *equivalent* LEFM provides an approximation of quasi-brittle fracture through the use of an equivalent linear elastic crack length (so called equivalent LEFM crack length) which gives, in a purely elastic medium, the same specimen stiffness as the one of the experimental specimen, *i.e.* the stiffness induced by the main crack with its FPZ [37,49,50].

Thus, a 3D numerical simulation was first built to simulate the crack propagation with the same geometry configuration as experimentally (see in Fig. 11) but assuming a purely linear elastic behavior described by Young modulus and Poisson ratio values respectively equal to 4.16 GPa [21] and 0.3. A symmetry plane was used and the crack propagation was done by releasing the nodes located in this plane. At each release of node, a numerical stiffness K was evaluated in the same way as experimentally by taking ratio between the nodal force at the pins and the displacement at the location where it is measured experimentally using the digital extensometers. Then, thanks to this simulation, the stiffness loss ratio which is the ratio between the current elastic stiffness and the initial one $\frac{K}{K_0}$ was calculated as a function of the crack length increment. The result is plotted in Fig. 12. This last relation was used to link the experimental stiffness at each cycle and the so-called equivalent LEFM crack length.

4. Final analysis

Based on the protocols explained in the previous section, eight tests (*i.e.* eight tablets) were performed and analyzed. The stiffness evolution for each cycle is plotted in Fig. 13. For all the tests, the initial stiffness exhibited a value around $1.2\,\mathrm{N\,\mu m^{-1}}$ with a deviation of 15%. The decrease was very well repeatable and the stiffness tended toward 0 at the cycle number 20.

Fig. 14 shows the results in terms of crack length increment ($\Delta a = a - a_0$) for the eight tests at each cycle in the same graphics than the experimental stiffness ratio obtained from the datas of Fig. 13. To get Δa, the data from Fig. 12 was used to derive, using an interpolation procedure, the value of the equivalent LEFM crack length increment from the experimental values of the stiffness loss ratio. The eight tests

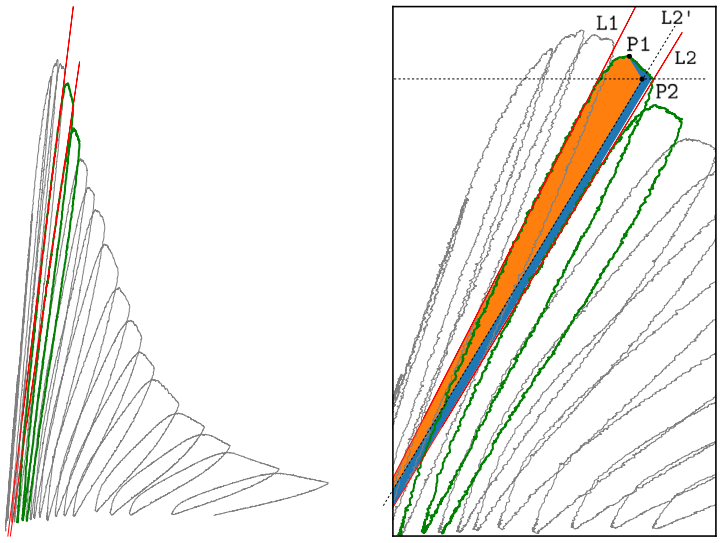

(a) 6-7

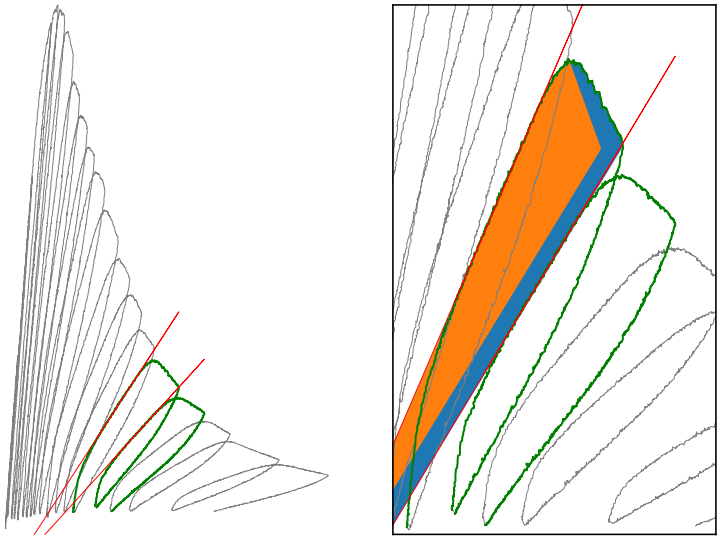

(b) 15-16

Fig. 10. Example of the energy dissociation for the sample #3, in between the cycles [6–7] and [15–16]. The orange area will be used as the elastic energy loss by damage and the blue area as the so-called 'plastic' energy loss by micro friction and/or micro plasticity. Red lines correspond to the initial elastic stiffnesses of each cycles.

showed the same tendency of a growing crack reaching a final crack length around 6 mm, close to the edge of the sample.

Thanks to the previous values for each test, the resistance to the equivalent LEFM crack growth noted G_R is plotted as a function of the crack length in Fig. 15-(a). G_R was obtained by dividing the so-called 'elastic' energy by the equivalent crack length increment and the width of the sample (4.6 mm), *i.e* the equivalent crack surface increment. An equivalent 'plastic' energy, noted as G_R^p, was also obtained by dividing the corresponding energy by the equivalent crack surface increment and plotted in Fig. 15-(b).

The G_R data showed an increasing tendency until reaching a constant value, which is a typical response observed in the case of quasi-brittle fracture. According to previous works [49,50], a fitting function was proposed to adjust the datas as:

$$G_R(\Delta a) = \begin{cases} G_{Rc}\left(\dfrac{\Delta a}{\Delta a_c}\right)^{\beta} & \text{if } \Delta a < \Delta a_c \\ G_{Rc} & \text{if } \Delta a \geq \Delta a_c \end{cases} \tag{2}$$

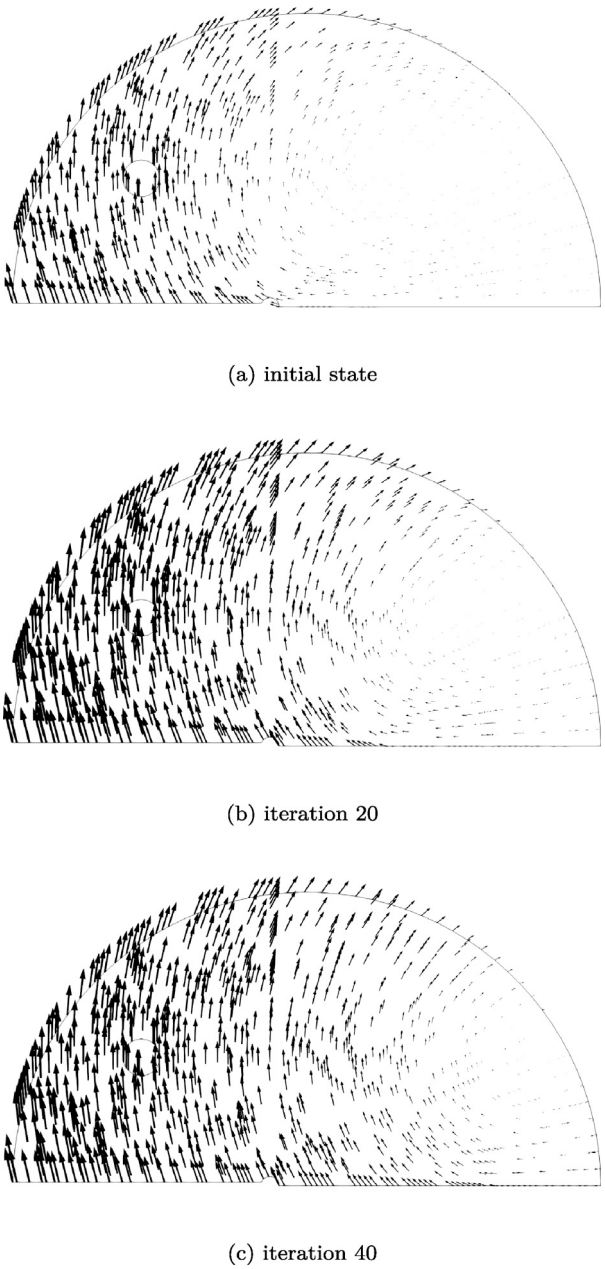

Fig. 11. Displacement field obtained by 3D FEM simulation.

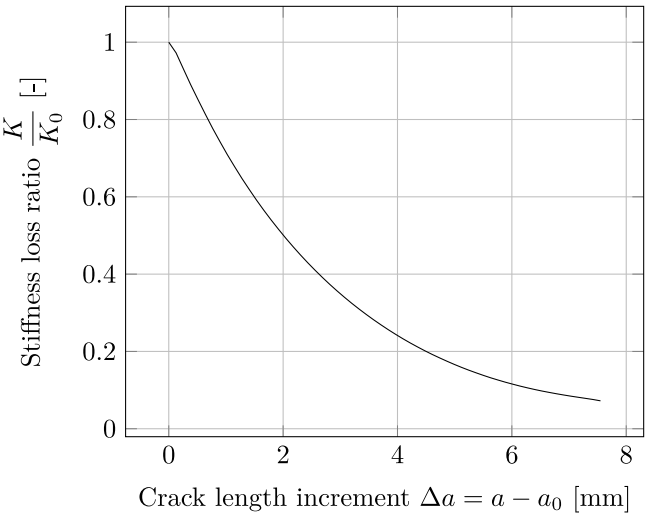

Fig. 12. Simulated loss ratio of the stiffness as a function of the crack length increment.

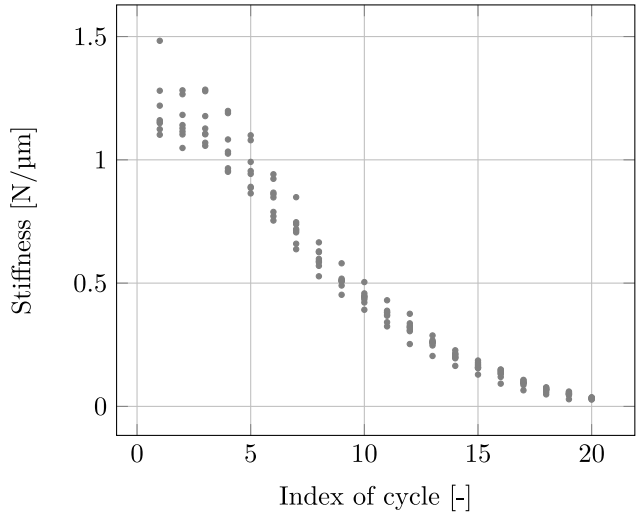

Fig. 13. Experimental results for the evaluation of the stiffness for all the 8 sample tested in this work.

where $\Delta a = a - a_0$ corresponds to the crack length increment from the initial notch length a_0, and $\Delta a_c = a_c - a_0$ is the critical crack length increment denoting the end of the rising part of the R-curve and so the onset of the plateau regime of the resistance to crack growth noted as G_{Rc} (a_c is then the eq. LEFM crack length for which G_{Rc} is reached). The β exponent guides the non linear rising of G_R. An incremental algorithm was built based on mean square method finding the optimal couple $\{\Delta a_c : \beta\}$ to minimize the mean square error. Thus, G_{Rc} took the value of the output coefficient of the mean square algorithm for this discontinuous function. The result is plotted as the blue dotted curve, noted 'fit', in Fig. 15-(a) with: $\Delta a_c = 2\,\text{mm}$, $\beta = 0.4081$ and $G_{Rc} = 4.68\,\text{J m}^{-2}$.

The R-curve data, *i.e.* the values of G_R as a function of Δa exhibited typical curve shape expected for a quasi-brittle material. The resistance to crack growth first increases before reaching a plateau value at a crack increment greater than Δa_c. The rising part of the R-curve (*i.e.* for $0 < \Delta a < \Delta a_c$) reflects the development of the FPZ from the initial notch to its maximum size at $\Delta a = \Delta a_c$. Thus, this critical crack length increment corresponds to the so called equivalent linear elastic length of the FPZ (eq. LEFM length of FPZ) which is approximately equal to 2 mm for ACP. The real length of the FPZ can be considered with a value between one and two times greater than its equivalent elastic length [37], but is nevertheless sufficiently small for this DCT geometry to guarantee a self-similar crack propagation.

For crack length increments $\Delta a > \Delta a_c$, the resistance to crack growth exhibits a plateau value G_{Rc} which emphasizes a self-similar crack propagation. This regime corresponds to the propagation of the main crack with its critical FPZ and this propagation takes place in a self-similar way emphasizing that the critical FPZ can be considered in an energetic steady state during the main crack propagation [37].

Moreover, for each tests, the equivalent crack length increment corresponding to the peak load, noted Δa_u was also evaluated with the same interpolation methods from the simulated stiffness loss ratio $\frac{K}{K_0}$, K being in this case the ratio $\frac{F_m}{d_u}$ (F_m and d_u being respectively the maximum load and its corresponding displacement) and are plotted in Fig. 15-(a) in green. All the values of Δa_u are around a mean value of 1.1 mm which is lower than the equivalent critical crack length

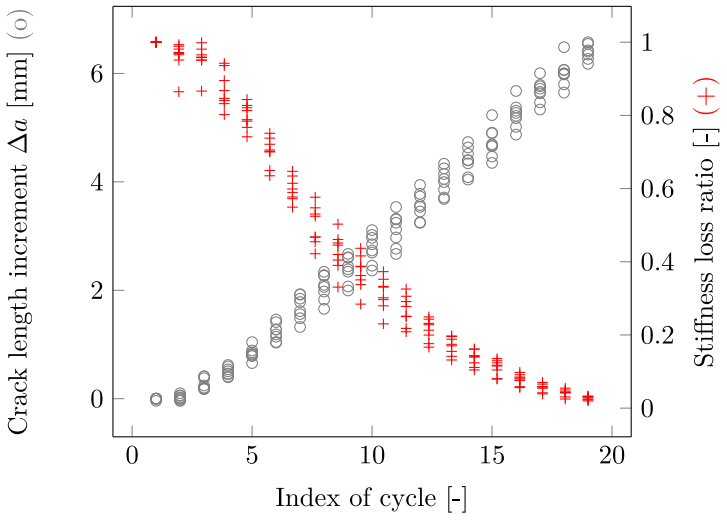

Fig. 14. Estimation of the crack length increment and the stiffness loss ratio for each cycles and for all the eight tested samples.

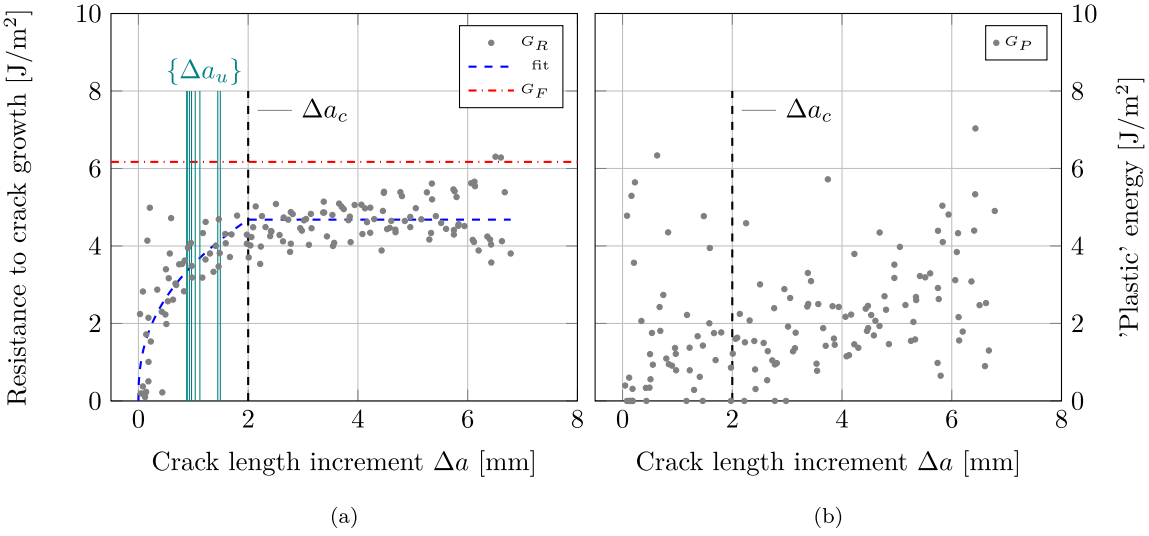

Fig. 15. Final R-curve for the ACP (a) and its corresponding 'plastic' energy curve (b).

increment Δa_c which indicates that the FPZ is not yet fully developed at the peak load with ACP.

Thus, the DCT test proposed in this work can be considered as valid in so far as it allows for (*i*) the self-similar propagation of the main crack with its FPZ (characterized by the plateau value of the R-curve) and, as a consequence, (*ii*) the free development of the FPZ from the initial notch preceeding this self-similar crack propagation. These two points are the two characteristics of a minimal dependence of the fracture process on the specimen geometry [37]

Moreover, the value G_{Rc} can be compared to the average fracture energy G_F of 6.17 J m^{-2} (the red dashed line in Fig. 15-(a)), which clearly shows and quantifies the contribution of other dissipative mechanisms during the fracture process for the ACP. Fig. 15-(b) represents the 'plastic' energy G_P associated with these other dissipative mechanisms. Despite the high variability of the data, one can see that the difference between G_F and G_R is of the same order of magnitude as G_P but not for all the data points, which can be one of the limits of the proposed protocol to indentify other dissipative mechanisms during a propagation. Numerical simulations at small scales could be a valuable benefit in this sense.

5. Discussion & conclusions

In the light of this experimental campaign, the material studied in this work reveals a quasi-brittle behavior in the sense that toughening non linear mechanisms are occurring at the crack tip inside a FPZ. Thus, the LEFM cannot be used without at least an adaptation such as the equivalent LEFM proposed here. Moreover, the peak load cannot also be used to build a design criteria. Indeed, for all tests of this campaign, the equivalent crack length increment at the peak load a_u was at most 60% of the critical equivalent crack length increment a_c (see Fig. 16). This critical value indicates the beginning of the self-similar regime that need to be captured experimentally to fully analyze the material. Fig. 16 illustrates this effect by putting the two corresponding stiffnesses for a_u and a_c on the data from Fig. 7. The green point indicates the end of the development of the FPZ and so the onset of the self-similar regime of the crack propagation.

Thus, the analysis of the fracture properties of the material from the peak load (which is the case of the brazilian's test) can only lead to a partial analysis of the fracture process. The characterization of the fracture properties of a quasi-brittle material requires the analysis

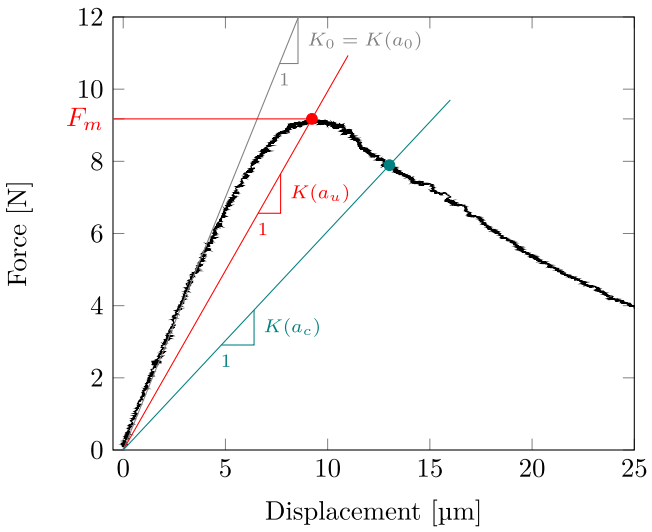

Fig. 16. Typical load–displacement curve obtained from a non-stabilized monotonic loading (sample #A).

of the whole fracture process (pre- and post-peak) and quantification of the evolution of the elastic stiffness of the specimen from loading–unloading cycles.

Moreover, these results show that in order to describe and simulate precisely the quasi-brittle behavior, it is necessary to use either a damage model [37] (softening) that can includes a plasticity part (in the case of ACP, it was shown that the 'plastic' energy cannot be neglected), or a discrete model also with softening but with a friction model instead of using a plasticity one, or again an analytical approach using the R-curve and the 'plastic' energy curve G_P given in this work.

Further fracture analyses on other classical materials coming from the pharmaceutical field are currently in process. As all of these materials are made by the same powder compaction process, it is expected that they will give also a quasi-brittle behavior and thus can be analyzed with the proposed methodology composed of:

- the stabilization of the Disk Shaped Compact Tension test using the notch opening displacement controller, that allows to avoid instability issues;
- the cycling loading in order to estimate the elastic stiffness evolution and thus to quantify all the other dissipative mechanisms like micro-friction inside the FPZ that can occur during the development of the FPZ and also during the self-similar regime;
- the equivalent LEFM framework which adapts the classical LEFM to the non linear case and where the resistance curve of the material can be obtained.

The perspective of this work is to build a featured cohesive law including the softening but also the micro-friction mechanisms. The implementation is now in process using very recent developments using the discrete element method [51] that will be able to simulate real application cases during the manufacturing process of the pharmaceutical tablets, such as capping or lamination.

CRediT authorship contribution statement

J. Girardot: Conceptualization, Methodology, Writing – review & editing, Supervision. **J.B. Kopp:** Supervision, Conceptualization. **B. Croquelois:** Methodology, Investigation. **P. Tchoreloff:** Funding acquisition. **S. Morel:** Supervision, Conceptualization. **V. Mazel:** Supervision, Conceptualization.

Declaration of competing interest

The authors declare the following financial interests/personal relationships which may be considered as potential competing interests: Vincent Mazel reports financial support was provided by French Agence Nationale de la Recherche.

Data availability

Data will be made available on request.

Acknowledgments

The authors acknowledge the support of the French Agence Nationale de la Recherche (ANR), under grant ANR-17-CE08-0015 (project CliCoPha). They are also deeply grateful for the implementation of the stabilized DCT test to Mr Bernard Solbes. The fracture tests have been performed on the Xyloplate platform equipments (Equipex XYLOFOREST - ANR-10-EQPX-16) also supported by the ANR, France.

References

[1] G. Alderborn, Tablets and compaction, in: Pharmaceutics - the Science of Dosage Form Design, Vol. 2, Churchill Livingstone, London, 2001.
[2] S. Garner, E. Ruiz, J. Strong, A. Zavaliangos, Mechanisms of crack formation in die compacted powders during unloading and ejection: An experimental and modeling comparison between standard straight and tapered dies, Powder Technol. 264 (2014) 114–127.
[3] E.N. Hiestand, J.E. Wells, C.B. Peot, J.F. Ochs, Physical processes of tableting, J. Pharm. Sci. 66 (4) (1977) 510–519.
[4] W.M. LONG, Radial pressures in powder compaction, Powder Metall. 3 (6) (1960) 73–86.
[5] V. Mazel, H. Diarra, J. Malvestio, P. Tchoreloff, Lamination of biconvex tablets: Numerical and experimental study, Int. J. Pharm. 542 (1) (2018) 66–71.
[6] V. Mazel, V. Busignies, H. Diarra, P. Tchoreloff, Lamination of pharmaceutical tablets due to air entrapment: Direct visualization and influence of the compact thickness, Int. J. Pharm. 478 (2) (2015) 702–704.
[7] V. Mazel, P. Tchoreloff, Lamination of pharmaceutical tablets: Classification and influence of process parameters, J. Pharm. Sci. 111 (5) (2022) 1480–1485.
[8] C.Y. Wu, B.C. Hancock, A. Mills, A.C. Bentham, S.M. Best, J.A. Elliott, Numerical and experimental investigation of capping mechanisms during pharmaceutical tablet compaction, Powder Technol. 181 (2) (2008) 121–129.
[9] X. Gong, C.C. Sun, A new tablet brittleness index, Eur. J. Pharmaceut. Biopharmaceut. 93 (2015) 260–266.
[10] A.T. Procopio, A. Zavaliangos, J.C. Cunningham, Analysis of the diametrical compression test and the applicability to plastically deforming materials, J. Mater. Sci. 38 (17) (2003) 3629–3639.
[11] M. Mellor, I. Hawkes, Measurement of tensile strength by diametral compression of discs and annuli, Eng. Geol. 5 (3) (1971) 173–225.
[12] T. Yanagidani, O. Sano, M. Terada, I. Ito, The observation of cracks propagating in diametrically-compressed rock discs, Int. J. Rock Mech. Min. Sci. Geomech. Abstr. 15 (5) (1978) 225–235.
[13] M. Thiercelin, J.C. Roegiers, Fracture toughness determination with the modified ring test, in: L. Chengxiang, Y. Ling (Eds.), Proceedings of the International Symposium on Engineering in Complex Rock Formations, Pergamon, 1988, pp. 284–290.
[14] L. Tutluoglu, C. Keles, Effects of geometric factors on mode I fracture toughness for modified ring tests, Int. J. Rock Mech. Min. Sci. 51 (2012) 149–161.
[15] M.P. Wagnoner, W.G. Buttlar, G.H. Paulino, Disk-shaped compact tension test for asphalt concrete fracture, Exp. Mech. 45 (3) (2005) 270–277.
[16] C.M. Stewart, C.W. Oputa, E. Garcia, Effect of specimen thickness on the fracture resistance of hot mix asphalt in the disk-shaped compact tension (DCT) configuration, Constr. Build. Mater. 160 (2018) 487–496.
[17] M.P. Wagnoner, W.G. Buttlar, G.H. Paulino, Disk-shaped compact tension test for asphalt concrete fracture, 45 (2005) 270–277.
[18] C.J. Gilbert, J.J. Cao, L.C. Jonghe, R.O. Ritchie, Crack-growth resistance-curve behavior in silicon carbide: small versus long cracks, 80 (2005) 2253–2261.
[19] H. Kim, M.P. Wagoner, W.G. Buttlar, Numerical fracture analysis on the specimen size dependency of asphalt concrete using a cohesive softening model, 23 (2009) 2112–2120.
[20] J.T. Fell, J.M. Newton, Determination of tablet strength by the diametral-compression test, J. Pharm. Sci. 59 (5) (1970) 688–691.
[21] V. Mazel, S. Guerard, B. Croquelois, J. Kopp, J. Girardot, H. Diarra, V. Busignies, P. Tchoreloff, Reevaluation of the diametral compression test for tablets using the flattened disc geometry, Int. J. Pharm. 513 (1–2) (2016) 669–677.

[22] I.C. Sinka, K.G. Pitt, A.C.F. Cocks, Chapter 22 the strength of pharmaceutical tablets, in: A.D. Salman, M. Ghadiri, M.J. Hounslow (Eds.), Handbook of Powder Technology, in: Particle Breakage, vol. 12, Elsevier Science B.V., 2007, pp. 941–970.
[23] G.E. Andreev, A review of the Brazilian test for rock tensile strength determination. Part I: calculation formula, Min. Sci. Technol. 13 (3) (1991) 445–456.
[24] G.E. Andreev, A review of the Brazilian test for rock tensile strength determination. Part II: contact conditions, Min. Sci. Technol. 13 (3) (1991) 457–465.
[25] D. Li, L.N.Y. Wong, The Brazilian disc test for rock mechanics applications: Review and new insights, Rock Mech. Rock Eng. 46 (2) (2013) 269–287.
[26] M.C.I.M. Amin, J.T. Fell, Tensile strength and bonding in compacts: A comparison of diametral compression and three-point bending for plastically deforming materials, Drug Dev. Ind. Pharm. 28 (2002) 809–813.
[27] J.L. Amorós, V. Cantavella, J.C. Jarque, C. Felíu, Green strength testing of pressed compacts: An analysis of the different methods, J. Eur. Ceram. Soc. 28 (4) (2008) 701–710.
[28] J. Hilden, M. Polizzi, A. Zettler, Note on the use of diametrical compression to determine tablet tensile strength, J. Pharm. Sci. 106 (1) (2017) 418–421.
[29] V. Mazel, H. Diarra, V. Busignies, P. Tchoreloff, Comparison of different failure tests for pharmaceutical tablets: Applicability of the Drucker–Prager failure criterion, Int. J. Pharm. 470 (1) (2014) 63–69.
[30] B. Croquelois, J. Girardot, J.B. Kopp, C. Cazautets, P. Tchoreloff, V. Mazel, Breaking pharmaceutical tablets with a hole: Reevaluation of the stress concentration factor and influence of the hole size, Powder Technol. 317 (2017) 126–132.
[31] B. Croquelois, J. Girardot, J.B. Kopp, P. Tchoreloff, V. Mazel, Quantification of tablet sensitivity to a stress concentration: Generalization of Hiestand's approach and link with the microstructure, Powder Technol. 369 (2020) 176–183.
[32] E.N. Landis, E.N. Nagy, D.T. Keane, Microstructure and fracture in three dimensions, Eng. Fract. Mech. 70 (7–8) (2003) 911–925.
[33] Z.P. Bažant, Analysis of work-of-fracture method for measuring fracture energy of concrete, J. Eng. Mech. 122 (2) (1996) 138–144.
[34] J.F. Labuz, S. Cattaneo, L.-H. Chen, Acoustic emission at failure in quasi-brittle materials, Constr. Build. Mater. 15 (5) (2001) 225–233.
[35] Z.P. Bažant, Concrete fracture models: testing and practice, Eng. Fract. Mech. 69 (2) (2002) 165–205.
[36] S. Morel, E. Bouchaud, J. Schmittbuhl, G. Valentin, R-curve behavior and roughness development of fracture surfaces, Int. J. Fract. 114 (4) (2002) 307–325.
[37] S. Morel, C. Lespine, J.L. Coureau, J. Planas, N. Dourado, Bilinear softening parameters and equivalent LEFM R-curve in quasibrittle failure, Int. J. Solids Struct. 47 (6) (2010) 837–850.
[38] T. Fett, D. Munz, R.D. Geraghty, K.W. White, Influence of specimen geometry and relative crack size on the R-curve, Eng. Fract. Mech. 66 (4) (2000) 375–386.
[39] L.E.T. Ferreira, T.N. Bittencourt, J.L.A.O. Sousa, R. Gettu, R-curve behavior in notched beam tests of rocks, Eng. Fract. Mech. 69 (17) (2002) 1845–1852.
[40] V. Busignies, P. Tchoreloff, B. Leclerc, C. Hersen, G. Keller, G. Couarraze, Compaction of crystallographic forms of pharmaceutical granular lactoses. II. Compacts mechanical properties, Eur. J. Pharmaceut. Biopharmaceut. 58 (3) (2004) 577–586.
[41] R.J. Roberts, R.C. Rowe, P. York, The measurement of the critical stress intensity factor (KIC) of pharmaceutical powders using three point single edge notched beam (SENB) testing, Int. J. Pharm. 91 (2) (1993) 173–182.
[42] T. Anderson, Fracture Mechanics, CRC Press, 2017.
[43] Y. Zhu, E.V. Dave, R. Rahbar-Rastegar, J.S. Daniel, A. Zofka, Comprehensive evaluation of low-temperature fracture indices for asphalt mixtures, Road Mater. Pavement Design 18 (sup4) (2017) 467–490.
[44] B. Croquelois, J.B. Kopp, J. Girardot, P. Tchoreloff, V. Mazel, Dynamic fracture analysis in Brazilian test: application to pharmaceutical tablets, Int. J. Fract. (2021).
[45] R.J. Roberts, R.C. Rowe, Brittle fracture propensity measurements on 'tablet-sized' cylindrical compacts, J. Pharm. Pharmacol. 38 (7) (1986) 526–528.
[46] F. Podczeck, J.M. Newton, The implications of the determination of the mechanical strength of powder compacts containing a pre-formed hole, Powder Technol. 132 (1) (2003) 10–15.
[47] O.A. Itiola, N. Pilpel, Formulation effects on the mechanical properties of metronidazole tablets, J. Pharm. Pharmacol. 43 (3) (1991) 145–147.
[48] C. Imbert, P. Tchoreloff, B. Leclerc, G. Couarraze, Indices of tableting performance and application of percolation theory to powder compaction, Eur. J. Pharmaceut. Biopharmaceut. 44 (3) (1997) 273–282.
[49] S. Morel, N. Dourado, G. Valentin, Wood : a quasibrittle material R-curve behavior and peak load evaluation, Int. J. Fract. 131 (4) (2005) 385–400.
[50] J.-L. Coureau, S. Morel, N. Dourado, Cohesive zone model and quasibrittle failure of wood: A new light on the adapted specimen geometries for fracture tests, Eng. Fract. Mech. 109 (2013) 328–340.
[51] M. Sage, J. Girardot, J.-B. Kopp, S. Morel, A damaging beam-lattice model for quasi-brittle fracture, Int. J. Solids Struct. 239–240 (2022) 111404.